



City Research Online

City, University of London Institutional Repository

Citation: Reyes-Aldasoro, C. C., Akerman, S. & Tozer, G. M. (2007). Measuring Red Blood Cell Velocity with a Keyhole Tracking Algorithm. Paper presented at the 11th Mediterranean Conference on Medical and Biological Engineering and Computing 2007, 26-06-2007 - 30-06-2007, Ljubljana, Slovenia. doi: 10.1007/978-3-540-73044-6_210

This is the accepted version of the paper.

This version of the publication may differ from the final published version.

Permanent repository link: <https://openaccess.city.ac.uk/id/eprint/4650/>

Link to published version: https://doi.org/10.1007/978-3-540-73044-6_210

Copyright: City Research Online aims to make research outputs of City, University of London available to a wider audience. Copyright and Moral Rights remain with the author(s) and/or copyright holders. URLs from City Research Online may be freely distributed and linked to.

Reuse: Copies of full items can be used for personal research or study, educational, or not-for-profit purposes without prior permission or charge. Provided that the authors, title and full bibliographic details are credited, a hyperlink and/or URL is given for the original metadata page and the content is not changed in any way.

City Research Online:

<http://openaccess.city.ac.uk/>

publications@city.ac.uk

Measuring Red Blood Cell Velocity with a Keyhole Tracking Algorithm

C.C. Reyes-Aldasoro¹, S. Akerman¹ and G.M. Tozer¹

¹ Cancer Research UK Tumour Microcirculation Group, Academic Unit of Surgical Oncology, Royal Hallamshire Hospital, The University of Sheffield, Sheffield, S10 2JF, U.K.

Abstract— A tracking algorithm is proposed to measure the velocity of red blood cells traveling through microvessels of tumors growing in skin flaps implanted on mice. The tracking is based on a keyhole model that describes the probable movement of a segmented cell between contiguous frames in a video sequence. When a history of movements exists, past, present and a predicted landing position define two regions of probability with a *keyhole* shape. This keyhole is used to determine if cells in contiguous frames should be linked to form tracks. Pre-processing segments cells from background and post-processing joins tracks and discards links that could have been formed due to noise or uncertainty. The algorithm presents several advantages over traditional methods such as kymographs or particle image velocimetry: manual intervention is restricted to the thresholding, several vessels can be analyzed simultaneously, algorithm is robust to noise and a wealth of statistical measures can be obtained. Two tumors with different geometries were analyzed; average velocities were 211 ± 136 [$\mu\text{m/s}$] (mean \pm std) with a range 15.9-797 [$\mu\text{m/s}$], and 89 ± 62 [$\mu\text{m/s}$] with a range 5.5-300 [$\mu\text{m/s}$] respectively, which are consistent with previous results in the literature.

Keywords— Red Blood Cell Tracking, Blood Velocity

I. INTRODUCTION

The analysis of red blood cell (RBCs) velocity is of interest in different areas like cochlear blood flow [1], cerebral microvessels [2] or tumor vasculature [3]. Despite its importance, the off-line measurement of velocity has been restricted to 1D or 2D cross-correlation or even manual measurements of distances over a screen [3]. Particle Image Velocimetry [4] (PIV) relies on the 2D cross-correlation between small windows of interest within an image which observe the relative movement of the intensities inside the window between frames. This analysis is restricted to simple geometries, like a single vessel or a branching point at the maximum since more complicated geometries could result in incorrect results due to aliasing or other artifacts. Kymographs [5] (sometimes called Space-Time Images) rely on 1D cross correlation of manually traced lines over an image in consecutive frames. This analysis is thus restricted to a single straight line and does not consider orientations but only relative movement.

In this paper tracking is understood as tracing the course or 2D movements of individual RBCs from frame to frame. For this purpose, RBCs need to be segmented and its positions identified. We then propose a tracking algorithm based on a keyhole model that describes the movement of RBCs that travel within the vasculature of tumors and links RBCs on contiguous frames to form tracks that span over the analyzed frames. The algorithm has minimal user intervention and is capable of analyzing complex vascular networks.

II. MATERIALS AND METHODS

A. Window chambers and RBC labeling

Window chambers were implanted on male SCID mice (12-16 week-old, 28-32g) under general anesthesia using i.p. injection of fentanyl citrate (0.8mgkg⁻¹) and fluanisone (10mgkg⁻¹; Hypnorm) and midazolam (5mgkg⁻¹; Hypnovel). Surgical procedures are described in [6]. Donor red blood cells were obtained by cardiac puncture from anaesthetized male SCID mice into heparinised syringe and labeled with the fluorescent dye DiI (Molecular Probes, Cambridge Biosciences, UK). The labeling method follows [7].

B. Intravital Microscopy

Intravital microscopy was carried out with an inverted Nikon Eclipse E600FN fluorescence microscope with a x2.5 zoom. The microscope was set up to view the tumor preparations under epi-fluorescence illumination using a 100 W mercury arc lamp for measurement of red blood cell velocity. Fluorescence was set up to excite at 550nm and detect the emissions at 565nm from the labeled red blood cells using a custom made fluorescence cube (Nikon, UK). Video observations were recorded in digital format, using a Sony DSR-30P digital videocassette recorder at 25 fps.

C. Description of the tracking algorithm

The tracking algorithm consisted of three main steps: *pre-processing* which transformed the acquired videos into a sequence of suitable binary images which contained segmented objects, *tracking*, which consisted of determining

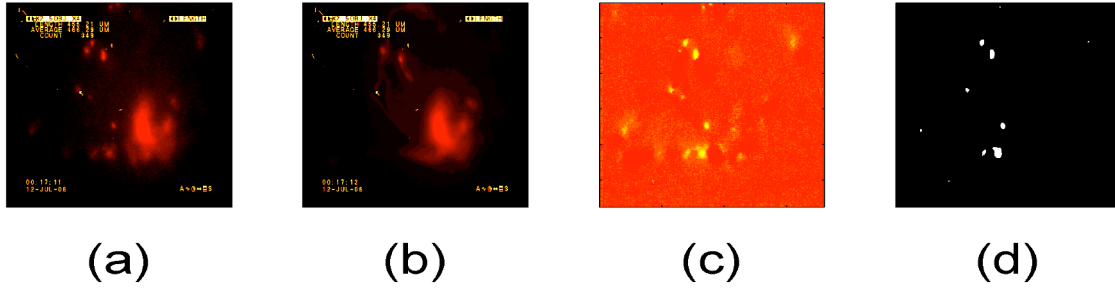


Fig. 2 Pre-processing of the images from input frames to binary images. (a) Sample frame where several RBC can be identified together with labels, noise and artifacts. (b) Mean image. (c) Pixel to pixel subtraction of (a) and (b). (d) Thresholded binary image of (c). 10 objects can be identified.

parent-child relationships between objects in contiguous frames, and *post-processing* which eliminated over-splitting of tracks and removed links that could have resulted from noise or uncertainty.

First, it was necessary to remove any artifacts, such as intensity inhomogeneity due to the acquisition process, noise, and all the labels that have been over-imposed on the images. A simple, yet powerful way of removing the artifacts is using a *mean image* [8], which was obtained by averaging the intensity values of every pixel of the image over all the frames to be analyzed. Then, this mean image was subtracted from every frame, removing most of the artifacts. To reduce the computational complexity and smooth the resulting images, a standard *Quad Tree* [9] averaging was performed. A quad tree averages the intensities of 4 neighboring pixels into a single one in a new image whose dimensions in rows and columns are half of the original. Besides the size reduction, local smoothing is performed. Next, a suitable threshold was selected to segment a number of *objects* (that is RBCs) from the background; this is the only manual intervention from the user (figure 2). Once the binary images were obtained, these were labeled, that is, assigned a unique label to each of the objects. Finally, the centroids of the objects were obtained together with the distances that separated them from its neighbors, if any.

We propose a *keyhole model* to perform the tracking of the RBCs. The model arose from the movements of RBCs: the most probable step for a RBC that is moving from frame $t-1$ to frame t , is to follow the direction of the previous steps with the same velocity to frame $t+1$. If we assume that a *child* RBC will move with exactly the same direction and velocity than its *parent*, we can predict its landing position for the next frame. Of course, this would not cover changes in speed, turns in vessels or even simple movements within a wide vessel. We therefore defined two regions of probability, a narrow wedge (60° wide) oriented towards the predicted landing position, and a truncated circle (300°) that complements the wedge, together resemble a keyhole

(figure 3). The radius of the wedge will be longer (3 x parent-child distance) than that of the circle (1 x parent-child distance) to capture objects that increased speed. The circle in turn would capture RBCs that changed direction but only those that are relatively close to the parent. In this way, parent-child relationships are restricted to objects that are relatively close to their parents or that follow the previous movements. This model can only be assumed if there is a previous history of movements of the RBCs, otherwise the only assumption is that the predicted landing of object will be within a certain distance of the former object, that is, a circular region centered at the parent. This of course introduces uncertainty in the relationship assigned, but this will be tested later in the post-processing. Once that all segmented RBCs have been examined for possible parent-child relationships, a reduced number of them will have formed a series of tracks of different lengths.

Post-processing consists of three steps: analysis of the first link, linking of disjoint tracks and removal of short tracks. First, for every track, the first RBC would have been assigned as a parent without any previous history of movements, thus it is possible that they were incorrectly assigned to the track. A simple way of ensuring that the top RBC, (time t) does belong to the track is analyzing the movement backwards, that is, apply the same keyhole model using child ($t+1$) and grandchild ($t+2$) to generate a keyhole. If the top RBC lands inside the keyhole, it remains as part of the track, otherwise it is removed. Next, in some cases, perhaps due to noise or incorrect segmentations, the path of a single RBC that would form 1 track can be split into 2. These tracks can be linked with a backwards analysis in a similar way as explained before. For every existing track, generate a keyhole with its top two RBCs, if the last node of another track lands within the keyhole, then link the tracks. The last post-processing step is to remove short tracks, those tracks that have more than 3 RBCs will be retained and the rest are removed under the assumption

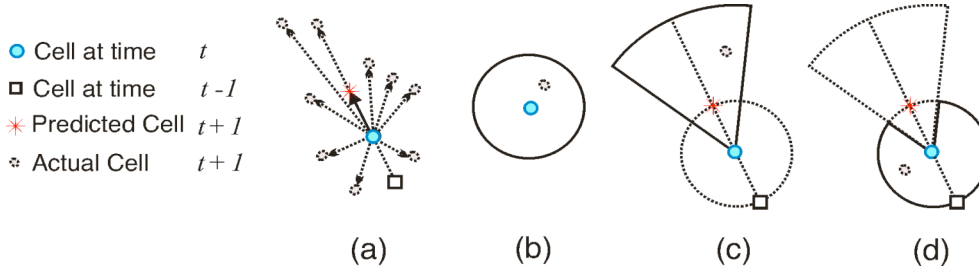


Fig. 3 RBC keyhole movement model. (a) It is assumed that between consecutive frames a RBC can move towards any direction any distance. (b) Without movement history, the only assumption possible is that its landing prediction will be within a circular region. (c, d) A predicted position is made assuming constant velocity and direction, this creates two probable regions a *cone* (c) and a *circle* (d) which when combined creates a *keyhole model*.

that they may have been generated by noise of the segmentation process.

III. RESULTS

The velocity of RBCs through two different tumors was analyzed, a series of tracks with their corresponding average velocities are presented in figure 4.

The vasculature can be observed clearly from the tracks together with the varying velocities of the RBCs that travel through the tumors. In figure 4 (a) it can be seen that there are several rather straight and narrow vessels with few curves, while in figure 4 (b) the majority of the RBCs travel through a wider vessel that reaches a branching point and then follow two different paths. At this branching point, the velocity of the RBCs increased significantly. In 4 (a) the velocity of different vessels can be quite different: a “fast” vessel can carry RBCs that travel at 500-700 [$\mu\text{m/s}$] (long straight on the left), while a “slow” vessel can have RBCs moving at 15-120 [$\mu\text{m/s}$] (“J” shaped in the top center). In 4 (b) the RBCs that travel through the main vessel present velocities in the range 170-300 [$\mu\text{m/s}$]. Since the tracks can have different lengths spanning from 4 to 172 frames, the mean value was obtained as a weighted average of their velocity by their length: $E(x) = \frac{\sum \text{Velocity}(i) \times \text{length}(i)}{\sum \text{length}(i)}$

where $E(x)$ is the expected value of the velocity, or its mean value and i , represents every track, and the standard deviation is: $std = \sqrt{E(x^2) - E(x)^2}$. The final velocity results (mean \pm std) for the two tumors are 211 \pm 136 [$\mu\text{m/s}$] with a range 15.9-797 [$\mu\text{m/s}$], and 89 \pm 62 [$\mu\text{m/s}$] with a range 5.5-300 [$\mu\text{m/s}$] respectively. These results are consistent with previous reports in the literature [3]. A further advantage of the tracking algorithm is that the tracks are inherently 3D vectors [rows x columns x time], and therefore they can be

plotted in different angles which can reveal information that is not visible in a traditional 2D time projection like the ones in figure 4. In figure 5, the tracks of the same tumors are presented with different view angles. First, in 5 (a) the tracks of the first tumor are presented in a “lateral” projection, where the vertical axis represents time going upwards and the horizontal axis represents the rows. This 2D plot is projected in a column plane. The time activity of the RBCs is highlighted in this view. Here, slow tracks will have a higher slope than the faster tracks that tend to be horizontal. There is even one RBC that seems to be trapped in its position and is represented by a vertical track that starts around second 8 on the left hand side of the graph. In figure 5 (b) we have selected a few tracks for clarity. It is now easier to distinguish the paths of the RBCs, most of which travel left-to-right, which would correspond down-up in figure 4 (a). Notice the RBC that changes direction in the middle of its path. Figure 5 (c) presents the tracks of the second tumor in a 3D plot where rows and columns form a base plane and time is going upwards. The majority of the RBCs travel through a wide vessels that then branches left and right. In figure 4 (b) all these tracks appear stacked on top of each other and its is hard to distinguish their paths. Some of the tracks on the left branch then change direction very abruptly. The tracks on the right-hand side are slower than those in the center.

Finally, since the movement between every frame is recorded for each RBC, it is possible to obtain a wealth of information, like angle and distance per frame, cumulative distance or distance from origin, not just average velocity.

IV. CONCLUSIONS

A tracking algorithm has been presented. The algorithm relies on a keyhole model that describes the probable movement of a red blood cell (RBC) through the vasculature of the vessels in tumors.

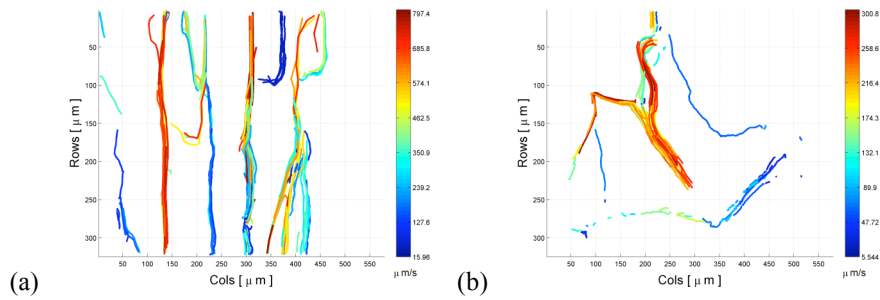


Fig. 4 Tracks obtained for two different tumors. Each individual RBC track is presented as a line with colors representing the velocities. It can be seen that the velocity in some vessels is consistently faster (red) than in others (blue). In (a) it is easy to notice how some vessels carry RBCs that travel much faster than in others, while in (b) the RBCs travel slower before the branching point and then accelerate in the separate branches.

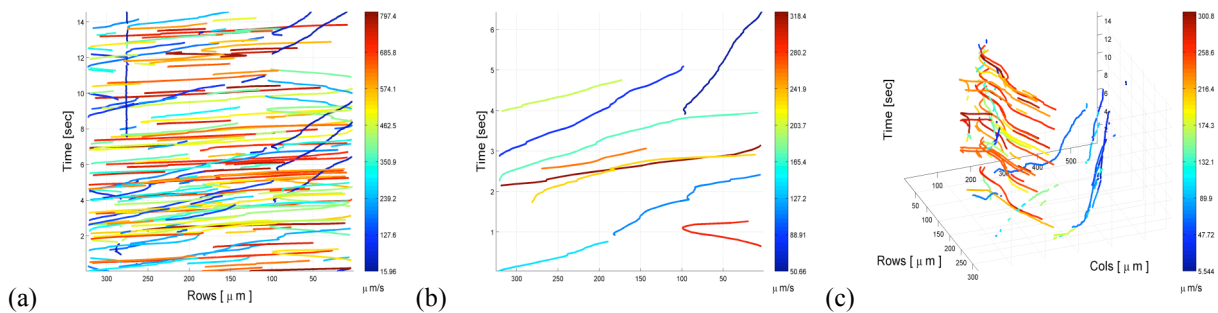


Fig. 5 Tracks from 2 tumors with different observation angles. While tracks in 4 are projected in time, tracks in (a) are projected in one column plane. Faster tracks will have lower slopes than slower tracks. (b) A reduced number of tracks from (a). Notice the track that changes direction in the middle of its path. (c) Tracks are presented in 3D with x-y dimensions (rows and columns) together with time in the z-axis.

The algorithm requires minimal user intervention and is able to track simultaneously RBCs in several straight or tortuous vessels without the use of cross-correlation. The results provide a wealth of information describing the movement of the RBC through the vasculature and not just the traditional mean and standard deviation of the velocity. A general aspect of geometry of the vessels of the tumor can also be observed. The algorithm has a series of noise reduction steps that provide better results.

REFERENCES

1. Prazma J, Carrasco VN, Garrett CG, Pillsbury HC. (1989). Measurement of cochlear blood flow: intravital fluorescence microscopy. *Hear Res* 42(2-3):229-36.
2. Tsukada K, Sekizuka E, Oshio C, Tsujioka K, Minamitani H. (2004). Red blood cell velocity and oxygen tension measurement in cerebral microvessels by double-wavelength photoexcitation. *J Appl Physiol* 96(4):1561-8.
3. Tozer GM, Prise VE, Wilson J, Cemazar M, Shan S, Dewhirst MW, Barber PR, Vojnovic B, Chaplin DJ. (2001). Mechanisms associated with tumor vascular shut-down induced by combretastatin A-4 phosphate: intravital microscopy and measurement of vascular permeability. *Cancer Res* 61:6413-6422.
4. Sugii Y, Nishio S, Okamoto K. (2002). In vivo PIV measurement of red blood cell velocity field in microvessels considering mesentery motion. *Physiol Meas* 23(2):403-16.
5. Waterman-Storer CM, Desai A, Bulinski JC, Salmon ED. (1998). Fluorescent speckle microscopy, a method to visualize the dynamics of protein assemblies in living cells. *Curr Biol* 8(22):1227-30.
6. Papenfuss HD, Gross JF, Intaglietta M, Treese FA. (1979). A transparent access chamber for the rat dorsal skin fold. *Microvasc. Res.* 18:311-318.
7. Unthank J, Lash J, Nixon J, Sidner R, Bohlen H. (1993). Evaluation of carbocyanine-labeled erythrocytes for microvascular measurements. *Microvascular Res* 45:193-210.
8. Japee SA, Ellis CG, Pittman RN. (2004). Flow visualization tools for image analysis of capillary networks. *Microcirculation* 11(1):39-54.
9. Gaede V, Günther O. (1998). Multidimensional access methods. *ACM Computing Surveys* 30(2):170-231.

Author: Constantino Carlos Reyes-Aldasoro
 Institute: The University of Sheffield
 Street: K Floor, Royal Hallamshire Hospital
 City: Sheffield
 Country: U.K.
 Email: c.reyes@sheffield.ac.uk